

# Copper(I) in the Cleft: Syntheses, Structures and Catalytic Properties of $\{\text{Cu}^+-\text{Co}^{3+}-\text{Cu}^+\}$ and $\{\text{Cu}^+-\text{Fe}^{3+}-\text{Cu}^+\}$ Heterobimetallic Complexes

Amit Pratap Singh<sup>[a]</sup> and Rajeev Gupta<sup>\*[a]</sup>

**Keywords:** Heterometallic complexes / Copper / Cobalt / Iron / Oxidation / Clefts

The present work demonstrates the synthesis and characterization of  $\{\text{Cu}^+-\text{Co}^{3+}-\text{Cu}^+\}$  and  $\{\text{Cu}^+-\text{Fe}^{3+}-\text{Cu}^+\}$  heterobimetallic complexes utilizing  $\text{Co}^{3+}$  and  $\text{Fe}^{3+}$  coordination complexes as the building blocks. The crystallographic investigation of the  $\{\text{Cu}^+-\text{Co}^{3+}-\text{Cu}^+\}$  and  $\{\text{Cu}^+-\text{Fe}^{3+}-\text{Cu}^+\}$  heterometallic complexes reveal that the  $\text{Cu}^{\text{I}}$  ions in the clefts are coordinated by two pyridine nitrogen atoms and one  $\text{CH}_3\text{CN}$  molecule. The crystal structures also show several weak interactions that result in interesting packing in the solid state. The ac-

cessible  $\text{Cu}^{2+/+}$  redox potential and presence of labile site on the copper center has been utilized for the oxidation of hindered phenols in the presence of molecular oxygen. Hindered phenols were oxidized to the C–C-coupled products in most cases, however, de-alkylation resulted in the case of 2,4,6-trisubstituted phenols. Interestingly, when  $\text{H}_2\text{O}_2$  was used as oxidant, de-alkylation was not observed; suggesting the uniqueness of the active species generated in the presence of catalyst and molecular oxygen.

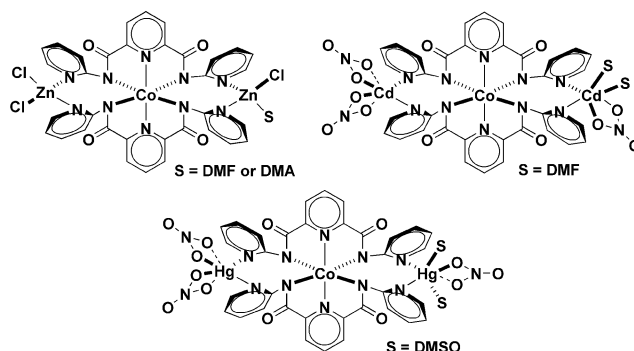
## Introduction

Remarkable progress has been made in the area of molecular inorganic–organic hybrid compounds. These compounds hold promise as new materials with novel catalytic, magnetic, electronic, and optical properties.<sup>[1]</sup> Versatile synthetic approaches for the assembly of such structures from the *building blocks* have been developed.<sup>[2]</sup> Considerable effort has been devoted to tune the building blocks as connectors and linkers in order to reach the stage of rational design with predictable architectures.<sup>[3]</sup> While most of the literature work is centered on placing a single metal ion in close proximity;<sup>[4]</sup> there are very few examples available where two different metal ions could be placed in close proximity in a step-wise fashion.<sup>[5]</sup> Such bi-metallic arrangements are extremely important for the synthesis of novel materials<sup>[5]</sup> and bi-functional catalysis.<sup>[6,7]</sup>

Our approach is to design, synthesize and utilize the coordination complexes as the building blocks for the construction of ordered structures where two different metal ions could be placed in close proximity.<sup>[8,9]</sup> A coordination complex as the building block offer many benefits such as spectroscopic and magnetic properties; and structural rigidity. Such an induced rigidity has the ability to place the auxiliary functional groups to a pre-organized conformation with an option to control the geometrical placement of the auxiliary functional groups. These auxiliary functional groups could then be utilized to coordinate a secondary

metal ion. This synthetic strategy may lead to the generation of the heterobimetallic complexes and networks of highly ordered nature.

The strategy described here uses a  $\text{M}^{3+}$  complex of the pyridine–amide ligands as the building block for the next-generation heterobimetallic systems.<sup>[8,9]</sup> The octahedral geometry of the  $\text{M}^{3+}$  ion orients the tethered pyridine rings with a definite directionality to coordinate a secondary metal ion, making suitable monomeric building blocks for preparing heterobimetallic complexes. Utilizing this strategy we have recently demonstrated the  $\text{Co}^{3+}$  coordination complex **1** as the building block for the preparation of  $\{\text{Zn}^{2+}-\text{Co}^{3+}-\text{Zn}^{2+}\}$ ,<sup>[8]</sup>  $\{\text{Cd}^{2+}-\text{Co}^{3+}-\text{Cd}^{2+}\}$ <sup>[9]</sup> and  $\{\text{Hg}^{2+}-\text{Co}^{3+}-\text{Hg}^{2+}\}$ <sup>[9]</sup> heterobimetallic complexes (Scheme 1). The selection of the peripheral metal ion was based on the possible application of the exposed Lewis acidic metal ion in organic transformations. Indeed, the Lewis-acidic property of the peripheral metal ion was demonstrated by the cata-



Scheme 1. Structurally characterized heterobimetallic complexes reported from our laboratory.

[a] Department of Chemistry, University of Delhi, Delhi 110007, India  
Fax: +91-11-2766-6605  
E-mail: rgupta@chemistry.du.ac.in

Supporting information for this article is available on the WWW under <http://dx.doi.org/10.1002/ejic.201000547>.

lytic organic transformation reactions such as the Beckmann rearrangement of the aldoximes and ketoximes; cyanosilylation reaction of imines, and ring-opening reactions of oxiranes and thiranes.<sup>[8,9]</sup> In order to further understand the coordinating abilities of such molecular clefts and their ability to accommodate assorted metal ions with variable coordination requirements, we were encouraged to look towards the Cu<sup>I</sup> metal ion. Extending the extremely modular approach, we report herein the synthesis and characterization of {Cu<sup>+</sup>–Co<sup>3+</sup>–Cu<sup>+</sup>} and {Cu<sup>+</sup>–Fe<sup>3+</sup>–Cu<sup>+</sup>} heterobimetallic complexes utilizing Co<sup>3+</sup> and Fe<sup>3+</sup> coordination complexes as the molecular building blocks. We then evaluate the effect of the central M<sup>3+</sup> metal on the structure and properties of the peripheral metal ion, Cu<sup>I</sup>. Further, the {Cu<sup>+</sup>–M<sup>3+</sup>–Cu<sup>+</sup>} heterobimetallic complexes are shown to take part in the oxidation of hindered phenols in the presence of molecular oxygen.

## Results and Discussion

**Building Blocks 1 and 2:** The Co<sup>3+</sup> and Fe<sup>3+</sup> complexes, Et<sub>4</sub>N[Co(L<sup>1</sup>)<sub>2</sub>] (**1**) and Et<sub>4</sub>N[Fe(L<sup>1</sup>)<sub>2</sub>] (**2**) have been used as the building blocks for the synthesis of heterobimetallic complexes. The synthesis and molecular structure of complex **1** has been recently reported by us.<sup>[8,10]</sup> The complex **2** was synthesized in an analogous manner and that involves reaction of the deprotonated ligand {L<sup>1</sup> = 2,6-bis[*N*-(2-pyridyl)carbamoyl]pyridine} with Fe<sup>II</sup> salt followed by the aerial oxidation to give the final Fe<sup>III</sup> product. Complex **2** was thoroughly characterized including crystallographic investigation. The molecular structure of the complex **2** is shown in Figure 1 whereas the bonding parameters are contained in Table 1. The unit cell contains two independent anionic molecules, two Et<sub>4</sub>N<sup>+</sup> cations and a water molecule. Both independent molecules show minor differences in the bonding parameters. The structure of complex **2** shows that two deprotonated tridentate ligands are arranged meridionally around the central iron metal via five-membered chelate rings between N<sub>amide</sub> and N<sub>pyridine</sub> atoms. Four deprotonated N<sub>amide</sub> atoms form the N<sub>4</sub> equatorial basal plane around the iron center while two N<sub>pyridine</sub> atoms occupy the axial positions. The Fe–N<sub>amide</sub> bond length is longer than the Fe–N<sub>pyridine</sub> by ca. 0.1 Å. The central N<sub>pyridine</sub> atoms are *trans* to each other and make an angle of ca. 175° with the central metal ion. The geometry around the central metal ion can be best described as the compressed octahedral as also noted for the complex **1**.<sup>[8]</sup> In both independent molecules, the hanging pyridine rings make angles of varying degrees with each other as well as with that of central pyridine ring. This suggests that the hanging pyridine rings are poorly pre-organized in absence of the secondary metal ions (Cu<sup>+</sup> ions, cf. crystal structures of **3** and **4**). A similar observation was noted for the analogous cobalt complex **1**.<sup>[8]</sup> The molecular structure of Fe<sup>3+</sup> complex **2** is very similar to that of Co<sup>3+</sup> complex, **1**<sup>[8]</sup> including the bond lengths, bond angles and geometry (see Table 1). The packing diagram of complex **2** shows interesting interactions between molecular

components (see Figure S1 in the Supporting Information). For example, the pyridine rings of two molecules were found to interact through weak C–H⋯C interactions that result in the formation of a two-dimensional (2D) layer. Two such 2D layers were connected to each other through the H-bonds between O<sub>amide</sub> atoms and the water molecule present as solvent of crystallization.

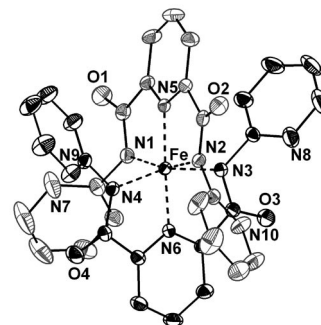


Figure 1. Molecular structure of building block **2**. Thermal ellipsoids are drawn at 50% level. Hydrogen atoms, cation, and a water molecule have been omitted for clarity. Two ligands are shown in black and grey for better understanding.

Table 1. Comparative bond lengths [Å] and bond angles [°] around the central M<sup>3+</sup> metal ion for complexes **1**, **2**, **3**, and **4**.

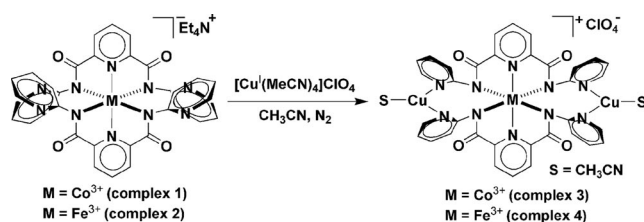
Bond <sup>[a]</sup>	<b>1</b> <sup>[b]</sup>	<b>2</b>	<b>3</b>	<b>4</b>
M–N1	1.998(7)	2.0327(18)	1.954(4)	1.964(4)
M–N2	1.962(8)	1.9554(19)	1.963(4)	1.964(4)
M–N3	2.048(7)	1.9832(19)	1.955(4)	1.972(5)
M–N4	1.935(8)	1.9568(19)	1.962(4)	1.963(5)
M–N5	1.872(7)	1.8931(18)	1.849(4)	1.864(5)
M–N6	1.870(7)	1.8885(18)	1.854(4)	1.882(5)
N1–M–N2	162.8(3)	161.11(8)	163.60(16)	162.73(19)
N3–M–N4	162.4(3)	161.39(8)	163.57(16)	162.53(19)
N2–M–N4	91.5(3)	91.33(8)	88.50(17)	89.05(18)
N1–M–N3	92.3(3)	92.95(8)	88.22(17)	88.84(19)
N5–M–N6	175.2(3)	175.33(8)	178.57(18)	178.20(2)

[a] M stands for Co<sup>3+</sup> for complexes **1** and **3**; and Fe<sup>3+</sup> for complexes **2** and **4**, respectively. [b] Ref.<sup>[8]</sup>

In both building blocks, **1**<sup>[8]</sup> and **2**, the central M<sup>3+</sup> ion is coordinated by two tridentate ligands in a meridional fashion. This coordination mode of the ligand however leaves two tethered pyridine rings un-coordinated or *hanging*. Such hanging pyridine rings from two ligands converge to form a cleft that has been shown to accommodate the Cu<sup>+</sup> ion to form {Cu<sup>+</sup>–Co<sup>3+</sup>–Cu<sup>+</sup>} (**3**) and {Cu<sup>+</sup>–Fe<sup>3+</sup>–Cu<sup>+</sup>} (**4**) heterobimetallic complexes (Scheme 2).

**Synthesis and Properties of {Cu<sup>+</sup>–Co<sup>3+</sup>–Cu<sup>+</sup>} (**3**) and {Cu<sup>+</sup>–Fe<sup>3+</sup>–Cu<sup>+</sup>} (**4**) Heterobimetallic Complexes:** The heterobimetallic complexes {Cu<sup>+</sup>–Co<sup>3+</sup>–Cu<sup>+</sup>} (**3**) and {Cu<sup>+</sup>–Fe<sup>3+</sup>–Cu<sup>+</sup>} (**4**) were synthesized by the reaction of **1** and **2** with [Cu(CH<sub>3</sub>CN)<sub>4</sub>]ClO<sub>4</sub> in CH<sub>3</sub>CN under the dinitrogen atmosphere (Scheme 2). The insertion of the Cu<sup>+</sup> ion immediately resulted in a distinct color change from deep green to yellow for complex **3** and red to deep brown for **4**. Complexes **3** and **4** were isolated as crystalline solid in >70% recrystallized yield. The FTIR spectra<sup>[11]</sup> of complexes **3** and **4** clearly show the stretches for the coordinated

CH<sub>3</sub>CN at ca. 2290 and 2253 cm<sup>-1</sup>. The proton NMR spectrum of complex **3** also showed the CH<sub>3</sub> protons of the coordinated CH<sub>3</sub>CN at  $\delta$  = 1.74 ppm. The  $\nu_{C=O}$  stretches for the amide group in the heterobimetallic complexes were found to be blue-shifted (15–39 cm<sup>-1</sup>) than their building block complexes. The conductivity measurements<sup>[12]</sup> of **3** and **4** in CH<sub>3</sub>CN show the 1:1 electrolyte nature. The absorption spectra for complexes **3** and **4** show the electronic transitions at 640 nm and 440 nm, respectively (Figure 2). The absorption spectra also show the changes incurred to the spectral features of the building block molecules after the insertion of secondary Cu<sup>+</sup> ion in the clefts (see Figures S2a and S2b in the Supporting Information). The solution state magnetic moment<sup>[13]</sup> of the {Cu<sup>+</sup>–Fe<sup>3+</sup>–Cu<sup>+</sup>} heterobimetallic complex was found to be 4.7  $\mu_B$  that fits well with an Fe<sup>III</sup> ion in an un-coupled environment. For comparison, the  $\mu_{eff}$  value for the building block **2** was found to be 4.6  $\mu_B$ .



Scheme 2. Synthesis of heterobimetallic complexes **3** and **4**.

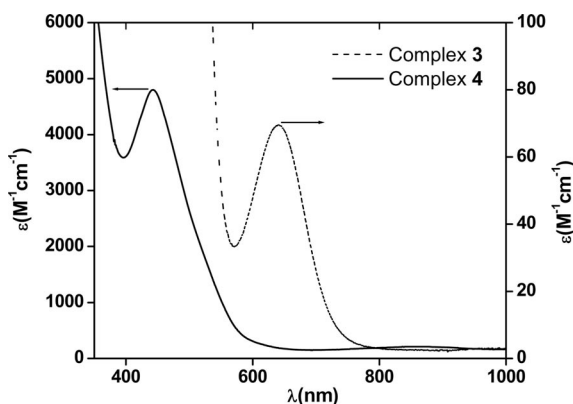


Figure 2. Comparison of the absorption spectra of heterobimetallic complexes **3** and **4** in CH<sub>3</sub>CN.

The diamagnetic nature of the complex **3** helped in the investigation of the solution state structure through <sup>1</sup>H and <sup>13</sup>C NMR spectra (Figure S3, Supporting Information). The signals were assigned via peak integration and comparison with the building block **1**. The most down-field signal at  $\delta$  = 8.13 ppm was assigned to the proton H<sup>9</sup> adjacent to the copper ion, which is ca. 0.35 ppm down-field shifted than the one for the building block **1**. Other pyridine ring proton signals were observed between  $\delta$  = 6.78–8.01 ppm. The <sup>13</sup>C NMR spectrum clearly showed nine signals for the nine chemically different carbon centers (Figure S3, Supporting Information).

**Crystal Structures of {Cu<sup>+</sup>–Co<sup>3+</sup>–Cu<sup>+</sup>} (**3**) and {Cu<sup>+</sup>–Fe<sup>3+</sup>–Cu<sup>+</sup>} (**4**) Heterobimetallic Complexes:** Both complexes **3** and **4** were crystallographically characterized and were found to be isostructural (Figure 3 and Figure 4). Two deprotonated tridentate ligands were arranged meridionally around the central M<sup>3+</sup> metal ion via five-membered chelate rings. The central M<sup>3+</sup> metal ion is coordinated by four deprotonated N<sub>amide</sub> atoms in the equatorial basal plane while two N<sub>pyridine</sub> atoms occupy the axial positions. The average M $\cdots$ N<sub>amide</sub> and M $\cdots$ N<sub>pyridine</sub> bond lengths were found to be little shorter than their respective building block molecules **1** and **2** (see Table 1). Crystal structures of the heterobimetallic complexes revealed that the central metal ion (Co<sup>3+</sup> in **3** and Fe<sup>3+</sup> in **4**) is geometrically unaffected by the insertion of the secondary copper(I) metal ion. Two Cu<sup>+</sup> metal ions are situated in the pre-organized *clefts* created by the hanging pyridine rings originated from the building block. Both secondary Cu<sup>+</sup> metal ions have trigonal-planar geometry, where two coordinations come from the hanging N<sub>pyridine</sub> atoms while the remaining one coordination is provided by the coordinated CH<sub>3</sub>CN molecule (Table 2). The average Cu $\cdots$ N<sub>CH<sub>3</sub>CN</sub> distance (1.951 Å and 1.965 Å for complexes **3** and **4**, respectively) is quite short than the similar distances reported in the literature.<sup>[14]</sup> The coordinated CH<sub>3</sub>CN molecules are almost linear (average CH<sub>3</sub>–CN bond angle is ca. 175° with deviation of less than ca. 5° from the ideal value of 180°). In both complexes, the

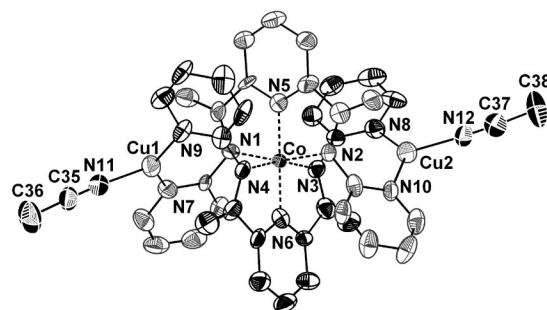


Figure 3. Molecular structure of heterobimetallic complex **3**. Thermal ellipsoids are drawn at 50% level. Hydrogen atoms and ClO<sub>4</sub><sup>-</sup> anion have been omitted for clarity. Two ligands are shown in black and grey for better understanding.

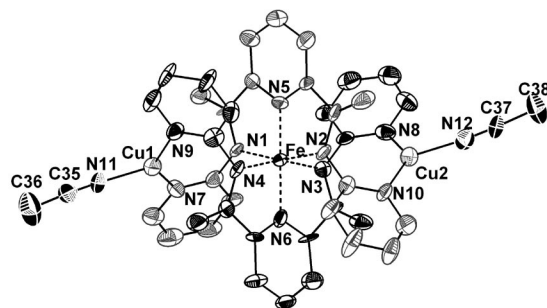


Figure 4. Molecular structure of heterobimetallic complex **4**. Thermal ellipsoids are drawn at 50% level. Hydrogen atoms and ClO<sub>4</sub><sup>-</sup> anion have been omitted for clarity. Two ligands are shown in black and grey for better understanding.



Cu<sup>I</sup> ion is almost within the trigonal plane defined by two pyridine nitrogen atoms and one CH<sub>3</sub>CN molecule with displacement in the range of 0.050–0.070 Å. Further, the sum of angles around the Cu<sup>I</sup> in both complexes is nearly 360° indicating a nearly perfect trigonal-planar geometry. For both complexes, the hanging pyridine rings are coordinated to the Cu<sup>I</sup> ion in dissecting form, making an angle in the range of ca. 40–42° with each other. The central and peripheral metal ions are placed almost linearly in both

Table 2. Comparative bond lengths [Å] and bond angles [°] around the peripheral Cu<sup>+</sup> ions for complexes **3** and **4**.

Bond	<b>3</b>	<b>4</b>
Cu1–N7	1.969(4)	1.971(5)
Cu1–N9	1.976(4)	1.975(5)
Cu1–N11	1.951(4)	1.967(5)
Cu2–N8	1.951(4)	1.963(5)
Cu2–N10	1.963(4)	1.963(5)
Cu2–N12	1.952(5)	1.962(5)
N7–Cu1–N9	131.49(17)	132.6(2)
N7–Cu1–N11	123.48(18)	123.2(2)
N9–Cu1–N11	104.83(18)	104.0(2)
N8–Cu2–N10	130.03(17)	130.7(2)
N8–Cu2–N12	112.49(18)	111.5(2)
N10–Cu2–N12	117.11(17)	117.5(2)

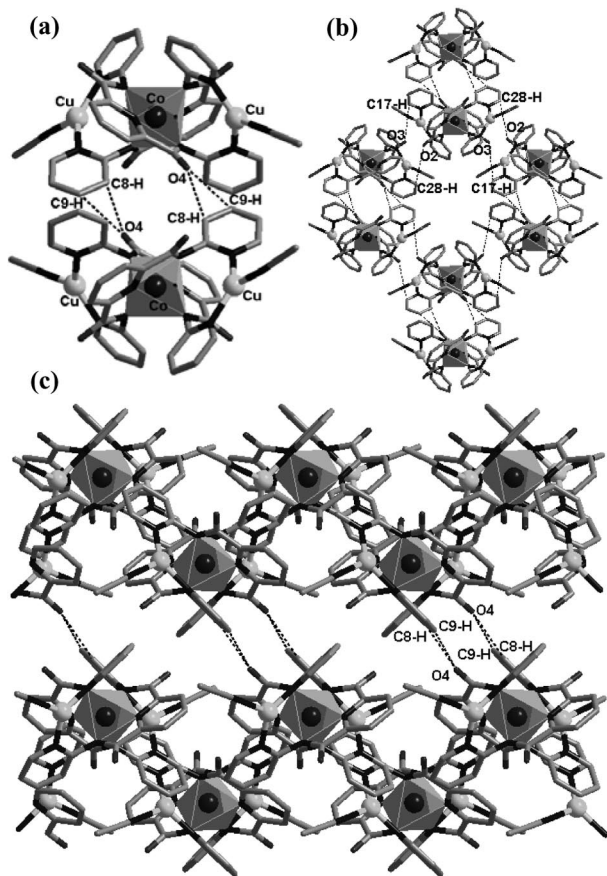


Figure 5. Weak interactions and packing diagram of complex **3**. Hydrogen atoms, anion, and a water molecule have been omitted for clarity. See text for details.

complexes making an angle of ca. 178.1°. The average Co...Cu and Fe...Cu distances are 4.183 Å and 4.177 Å, respectively.

Both complexes **3** and **4** show various kinds of weak interactions (Figure 5 and Figure 6). Two individual molecules were found to be involved in weak C–H...O hydrogen bonds resulting in the formation of an oval-shaped dimer. In addition, these dimers are further connected through the intermolecular hydrogen bonds that results in an interesting packing. For a dimer, two molecules are inter-connected via H-bonds between amide atom O4 and two pyridine C–H protons, C8–H and C9–H. The heteroatom separations, O4...C8 and O4...C9 were found to be 2.987 Å and 2.936 Å (for complex **3**); and 2.948 and 2.985 Å (for complex **4**), respectively. Further, these dimers are also connected to each other via two H-bonds between O2...C28–H and O3...C17–H with heteroatom separation of 3.332 Å and 3.304 Å (for complex **3**), and 3.326 and 3.310 Å (for complex **4**), respectively, to form a 2D network when viewed along the *c*-axis.

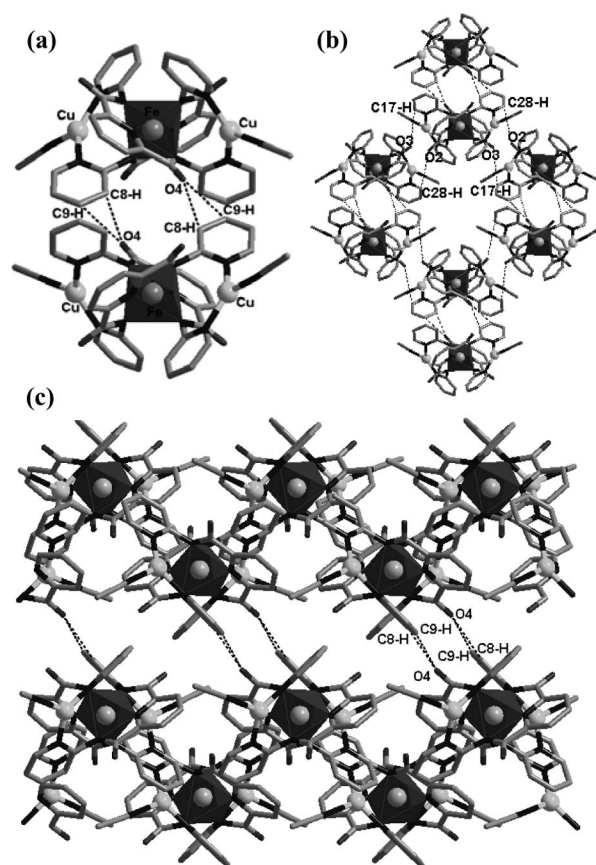


Figure 6. Weak interactions and packing diagram of complex **4**. Hydrogen atoms, anion, and a water molecule have been omitted for clarity. See text for details.

**Thermal Analysis:** To gain an insight about the thermal stability of the complexes **3** and **4** in general and coordinated CH<sub>3</sub>CN in particular, differential scanning calorimetry (DSC) and thermal gravimetric analysis (TGA) studies

were performed (Figures S4a and S4b, Supporting Information). DSC plots were recorded in the temperature range of 25–400 °C. The analysis showed that the coordinated solvent molecules, CH<sub>3</sub>CN were removed in the endothermic region in the temperature range of 70–80 °C (For complex **3**, thermal gravimetric analysis: obsd. weight loss: 7.96%, calcd. weight loss: 8.19%). DSC analysis also revealed that both complexes were thermally stable up to ca. 350 °C. The melting temperature ( $T_M$ ) for complexes **3** and **4** were found to be 340 and 350 °C, respectively.

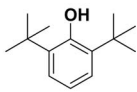
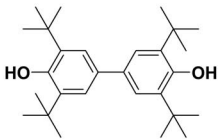
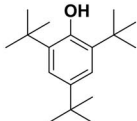
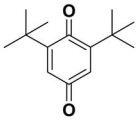
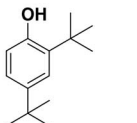
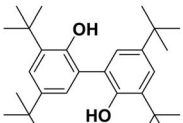
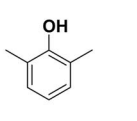
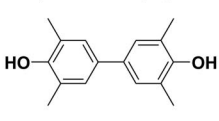
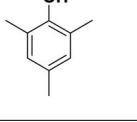
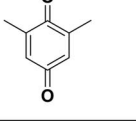
**Electrochemical Studies:** To investigate the redox behavior of the coordinated Cu<sup>I</sup> ions within the cleft of the building block and the extent of stabilization of the central metal ion towards reduction, cyclic voltammetric studies were performed. Cyclic voltammograms of complexes **3** and **4** in CH<sub>3</sub>CN solution at a glassy carbon electrode show a one-electron Cu<sup>2+/+</sup> irreversible reductive response with  $E_{pc}$  values of –0.59 V and –0.68 V vs. SCE, respectively (Figure S5a, Supporting Information). The redox potentials indicate that the molecular clefts stabilize the +2 state of the copper ions present in the clefts to a considerable extent. Such a negative potential also suggest that the Cu<sup>I</sup> ions will be able to activate molecular oxygen. An additional irreversible oxidative response ( $E_{pa}$ ) for complexes **3** and **4** was obtained at 1.66 and 1.68 V, respectively, that we tentatively assign as the one electron oxidation of the heterobimetallic complexes (Figure S5b, Supporting Information). We postulate that the locus of this oxidation is within the building block based on the literature precedents for similar type of complexes.

**Oxidation of Hindered Phenols:** The observation of Cu<sup>2+/+</sup> redox potential at negative value suggest that the copper ions present in the clefts have the tendency to stabilize the +2 oxidation state to a greater extent. It has been suggested that the Cu<sup>I</sup> species containing labile sites with an accessible Cu<sup>II</sup> oxidation state display oxidation properties towards the externally added substrates.<sup>[15–18]</sup> This prompted us to probe possible substrate oxidation reactions using molecular oxygen as the sole oxidant. The ability of copper containing metalloproteins and synthetic metal complexes to oxidize the hindered phenols has been the focus of continued interest in bioinorganic chemistry.<sup>[15,16]</sup> The oxidative coupling reaction of substituted phenols constitutes an interesting research topic both from the biological<sup>[18]</sup> and synthetic standpoints.<sup>[15]</sup> For example, aerobic oxidation of 2,6-dimethylphenol with copper(I) salt in the presence of N-donor ligands produces a *p*-phenylene oxide polymer which is widely used as an engineering thermoplastic under the trade name PPO.<sup>[19]</sup> Further, the enzyme tyrosinase also oxidizes the externally added substituted phenols to the coupled products in the absence of a suitable substrate.<sup>[20]</sup> The oxidation of hindered phenols by copper complexes are important as they provide an alternate route to cleaner products using molecular oxygen in place of toxic oxidizing agents.<sup>[21]</sup> The product selectivity depends upon the substitution present on the phenol and the mechanism of the oxidation.<sup>[21]</sup> Both {Cu<sup>+</sup>–Co<sup>3+</sup>–Cu<sup>+</sup>} and {Cu<sup>+</sup>–Fe<sup>3+</sup>–Cu<sup>+</sup>} heterobimetallic complexes were

tested for the oxidation of hindered phenols in the presence of molecular oxygen as the sole oxidant. All catalytic reactions were carried out in CH<sub>3</sub>OH or CH<sub>3</sub>CN and the results are summarized in Table 3. For 2,6-di-*tert*-butylphenol, carbon–carbon coupled product, 3,5,3',5'-tetra-*tert*-butylbiphenyl-4,4'-diol was obtained due to the coupling at the *para* position (entry 1). However, 2,4-di-*tert*-butylphenol gave a similar carbon–carbon-coupled product, 3,5,3',5'-tetra-*tert*-butylbiphenyl-2,2'-diol after the coupling at the *ortho* position (entry 3). Similar results were observed in the case of methyl-substituted phenol, for example, 2,6-dimethylphenol produced 3,5,3',5'-tetramethylbiphenyl-4,4'-diol as the *para* coupled product (entry 4). In case of 2,4,6-trisubstituted phenols (entries 2 and 5), the addition of base was found to be necessary to start the reaction. We believe that it generates the corresponding phenolate anion by dissociating the acidic proton, which is known to be more oxidizable than the phenol itself because of the difference between their redox potentials.<sup>[15b]</sup> In both these cases, dealkylation took place that resulted in the formation of the corresponding *p*-benzoquinones, 2,6-di-*tert*-butyl-1,4-benzoquinone (entry 2) and 2,6-dimethyl-1,4-benzoquinone (entry 5). Interestingly, in case of 2,4,6-tri-*tert*-butylphenol, *tert*-butyl alcohol was also observed in quantitative yield suggesting the homolytic cleavage of the carbon–carbon bond. Similarly, methyl alcohol is expected in the oxidation reaction of 2,4,6-trimethylphenol, however, its formation was not established as solvent used was also CH<sub>3</sub>OH. In the literature, a similar de-alkylation reaction of 2,4,6-tri-*tert*-butylphenol mediated by the copper complex and molecular oxygen has been reported.<sup>[22]</sup> However, the *tert*-butyl group was found to be de-alkylated both at the *ortho*- and *para*-positions producing 2,6-di-*tert*-butyl-1,4-benzoquinone and 4,6-di-*tert*-butyl-1,2-benzoquinone.<sup>[22]</sup> In the present case, the de-alkylation reaction took place only at the *para*-position. We tentatively propose that the substituted phenol is able to approach the copper center present in the cleft from one direction only and the *ortho*-position was protected and the reaction (radical generation and de-alkylation) took place at the remote *para*-position.

The catalytic reactions were also attempted in CH<sub>3</sub>CN as solvent. A trace amount of product was observed in most of the cases when molecular oxygen was used as the oxidant. However, when the oxidation was carried out using H<sub>2</sub>O<sub>2</sub>, a small amount (10–45%, entries 1, 3, and 4) of the carbon–carbon coupled products were obtained in case of 2,4-di-*tert*-butylphenol, 2,6-dimethylphenol and 2,6-di-*tert*-butylphenol. Interestingly, no de-alkylation product was noticed when H<sub>2</sub>O<sub>2</sub> was used as the oxidizing agent either in CH<sub>3</sub>OH or CH<sub>3</sub>CN. These results clearly pinpoint that the nature of the active oxidizing species generated in the reaction while using O<sub>2</sub> and H<sub>2</sub>O<sub>2</sub> are different. We speculate that in case of H<sub>2</sub>O<sub>2</sub> catalyzed reactions, a radical pathway takes place where the role of the {Cu<sup>+</sup>–M<sup>3+</sup>–Cu<sup>+</sup>} heterobimetallic complexes is rather limited. However, when the oxidation reaction was carried out in the presence of molecular oxygen, a unique catalytic species generates and causes the de-alkylation of the substituted phenols.

Table 3. Oxidation of substituted phenols with catalysts **3** and **4**.<sup>[a]</sup>

Entry	Substrate	Product	Solvent	Yield <sup>[b]</sup> (TON) with catalyst <b>3</b>	Yield <sup>[b]</sup> (TON) with catalyst <b>4</b>
1			CH <sub>3</sub> OH CH <sub>3</sub> CN <sup>[c]</sup>	81(16) 40	85(17) 45
2 <sup>[d]</sup>			CH <sub>3</sub> OH CH <sub>3</sub> CN <sup>[c]</sup>	80(16) n.r. <sup>[e]</sup>	93(19) n.r. <sup>[e]</sup>
3			CH <sub>3</sub> OH CH <sub>3</sub> CN <sup>[c]</sup>	24(5) 8	45(9) 10
4			CH <sub>3</sub> OH CH <sub>3</sub> CN <sup>[c]</sup>	80(16) 25	90(18) 30
5 <sup>[d]</sup>			CH <sub>3</sub> OH CH <sub>3</sub> CN <sup>[c]</sup>	70(14) n.r. <sup>[e]</sup>	82(16) n.r. <sup>[e]</sup>

[a] Reaction condition: catalyst: 5 mol-%, time: 6 h stirring at room temperature in the presence of O<sub>2</sub> atmosphere. [b] Isolated yield. [c] Reaction was done in CH<sub>3</sub>CN with H<sub>2</sub>O<sub>2</sub> as oxidant. [d] An equimolar amount of NaOH was used in the reaction. [e] n.r.: no reaction.

A similar oxidation reaction was also attempted using 9,10-dihydroanthracene (DHA) as substrate. DHA provides two weak C–H bonds<sup>[23]</sup> (bond dissociation energy: 78 kcal/mol) and has been used to distinguish the mode of oxidation, C–H vs. O–H activation. No reaction took place when DHA was used as the substrate in the presence of catalysts **3** or **4** under identical experimental conditions, either using molecular oxygen or H<sub>2</sub>O<sub>2</sub> as the oxidants. This clearly suggests that the catalysts activate the O–H bonds in the presence of molecular oxygen despite the stronger bond strength of the O–H bond in phenol (bond dissociation energies for phenol<sup>[24]</sup> and 2,4,6-tri-*tert*-butylphenol<sup>[25]</sup> are 90 and 81 kcal/mol, respectively). We tentatively provide a rationale for the observed reactivity. First, the in-situ generated Cu<sup>II</sup> reacts with phenol in acid–base mechanism and the resulted Cu<sup>2+</sup>–OPh adduct undergoes the homolysis to provide the phenoxyl radical and the Cu<sup>I</sup> species.<sup>[26]</sup> The Cu<sup>I</sup> species again oxidizes to Cu<sup>II</sup> in the presence of dioxygen and thus generates superoxide radical.<sup>[22]</sup> On the other hand, the phenoxyl radical gives rise to the carbon–carbon coupled product. For the de-alkylation reaction, we believe that the in-situ generated superoxide radical attacks the rearranged phenoxyl radical to produce an intermediate hydroperoxy compound, which rapidly eliminates a molecule of *tert*-BuOH (observed as the by-product in GC-MS analysis) to give the *p*-benzoquinone as the product. As can be seen from the Table 3, complex **4** dis-

plays better conversion of the substrates to the corresponding products over complex **3**. This difference in the catalytic activity can probably be attributed to the difference in the central metal ion and its effect on the redox potential and thus catalytic performance of the peripheral metal ion.

## Conclusions

The synthesis and characterization of {Cu<sup>+</sup>–Co<sup>3+</sup>–Cu<sup>+</sup>} and {Cu<sup>+</sup>–Fe<sup>3+</sup>–Cu<sup>+</sup>} heterobimetallic complexes utilizing Co<sup>3+</sup> and Fe<sup>3+</sup> coordination complexes as the building blocks is described. The insertion of the Cu<sup>I</sup> ion into the molecular clefts does not cause structural distortion of the building block, which attests the flexibility and accommodativity of the building blocks in accepting the assorted metal ions. The crystallographic investigations of the {Cu<sup>+</sup>–Co<sup>3+</sup>–Cu<sup>+</sup>} and {Cu<sup>+</sup>–Fe<sup>3+</sup>–Cu<sup>+</sup>} heterobimetallic complexes reveal that the Cu<sup>I</sup> ion in the clefts are coordinated by two pyridine nitrogen atoms and one CH<sub>3</sub>CN molecule. The crystal structures also show several weak interactions that result in interesting packing in the solid state. The accessible Cu<sup>2+/+</sup> redox potential and presence of labile site on the metal center has been utilized for the oxidation of hindered phenols in the presence of molecular oxygen. Hindered phenols are oxidized to give C–C-coupled products in most cases, however, de-alkylation results in the case of



2,4,6-trisubstituted phenols. Interestingly, when  $\text{H}_2\text{O}_2$  is used as oxidant, de-alkylation is not observed. This finding proves the uniqueness of the active species generated in the presence of catalyst and molecular oxygen.

## Experimental Section

**Materials and Reagents:** The solvents were purified as reported in ref.<sup>[27–31]</sup> The ligand  $\text{H}_2\text{L}^1$  and complex  $\text{Et}_4\text{N}[\text{Co}(\text{L}^1)_2]$  (**1**) were synthesized according to our earlier reports.<sup>[8,10]</sup>  $[\text{Fe}(\text{MeCN})_4](\text{ClO}_4)_2$  and  $[\text{Cu}(\text{CH}_3\text{CN})_4](\text{ClO}_4)$  salts were prepared following the literature procedures.<sup>[32]</sup>

### Syntheses

**$\text{Et}_4\text{N}[\text{Fe}(\text{L}^1)_2]\cdot\text{H}_2\text{O}$  (**2**):** A mixture of  $[\text{Fe}(\text{MeCN})_4](\text{ClO}_4)_2$  (328 mg, 0.78 mmol), ligand  $\text{H}_2\text{L}^1$  (500 mg, 1.56 mmol) and  $\text{K}_2\text{CO}_3$  (5.40 g, 39.14 mmol) in  $\text{CH}_3\text{CN}$  was refluxed for 4 h. The reaction produced a red coloured solution. After that  $\text{Et}_4\text{NCl}\cdot x\text{H}_2\text{O}$  (390 mg, 2.35 mmol) was added and the resulting reaction mixture was further stirred for 2 h at room temperature in open air. This resulted in a deep red colored solution. The solution was filtered and the volatiles were removed under reduced pressure to afford the crude product. Recrystallization was achieved by the slow diffusion of the vapors of diethyl ether to a  $\text{CH}_3\text{CN}$  solution of the crude product at room temperature. This afforded red-colored crystalline product suitable for the X-ray analysis; yield 0.44 g (69%).  $\text{C}_{42}\text{H}_{42}\text{FeN}_{11}\text{O}_4\cdot\text{H}_2\text{O}$  (838.28): calcd. C 60.15, H 5.29, N 18.37; found C 60.05, H 5.50, N 18.25. FTIR spectrum (KBr disk):  $\tilde{\nu} = 1590$  ( $\text{C}=\text{O}$ )  $\text{cm}^{-1}$ . Conductivity ( $\text{CH}_3\text{CN}$ , ca. 1 mM solution, 298 K):  $\Lambda_{\text{M}} = 140 \text{ } \Omega^{-1}\text{cm}^2\text{mol}^{-1}$ . UV/Vis spectrum (MeCN):  $\lambda_{\text{max}}$  ( $\epsilon$ ,  $\text{M}^{-1}\text{cm}^{-1}$ ) = 441 (5250) nm. ESI-MS ( $\text{CH}_3\text{CN}$ ):  $m/z = 821.064$  [ $\text{M} + \text{H}^+$ ].  $\mu_{\text{eff}}$  (DMF, 298 K, Evans' method): 4.6 BM.

**$[\text{Co}(\text{L}^1)_2\text{--}\{\text{Cu}(\text{CH}_3\text{CN})_2\}](\text{ClO}_4)$  (**3**):** To a solution of  $\text{Et}_4\text{N}[\text{Co}(\text{L}^1)_2]$  (**1**) (0.100 g, 0.121 mmol) in 20 mL of  $\text{CH}_3\text{CN}$ ,  $[\text{Cu}(\text{CH}_3\text{CN})_4](\text{ClO}_4)$  (0.079 g, 0.2428 mmol) was added under dinitrogen atmosphere. A colour change from green to light yellow was observed. The resultant reaction mixture was stirred for 1 h. The solution was filtered and the volatiles were removed under reduced pressure to afford a yellow coloured product. The recrystallization was achieved by the slow vapour diffusion of diethyl ether to a  $\text{CH}_3\text{CN}$  solution of the crude compound at room temperature; yield 0.085 g (70%).  $\text{C}_{38}\text{H}_{28}\text{ClCoCu}_2\text{N}_{12}\text{O}_8$  (1002.19): calcd. C 44.74, H 2.98, N 16.48; found C 44.55, H 3.03, N 16.33. FTIR spectrum (KBr disk):  $\tilde{\nu} = 2286, 2253, 1616, 1594, 1089 \text{ cm}^{-1}$ . Conductivity ( $\text{CH}_3\text{CN}$ , ca. 1 mM solution, 298 K):  $\Lambda_{\text{M}} = 125 \text{ } \Omega^{-1}\text{cm}^2\text{mol}^{-1}$ . UV/Vis spectrum ( $\text{CH}_3\text{CN}$ ):  $\lambda_{\text{max}}$  ( $\epsilon$ ,  $\text{M}^{-1}\text{cm}^{-1}$ ): 640 (70), 470 (sh, 1900) nm.  $^1\text{H}$  NMR spectrum (300 MHz,  $\text{CD}_3\text{CN}$ , 25 °C):  $\delta = 8.13$  (d,  $J = 6.3$  Hz, 4 H,  $\text{H}^9$ ), 8.01 (t,  $J = 6.5$  Hz, 2 H,  $\text{H}^1$ ), 7.67 (d,  $J = 7.8$  Hz, 4 H,  $\text{H}^2$ ), 7.15 (t,  $J = 6.4$  Hz, 4 H,  $\text{H}^7$ ), 7.08 (t,  $J = 6.4$  Hz, 4 H,  $\text{H}^8$ ), 6.78 (d,  $J = 6.4$  Hz, 4 H,  $\text{H}^6$ ), 1.74 (6H- $\text{CH}_3$   $\text{CH}_3\text{CN}$ ) ppm.  $^{13}\text{C}$  NMR spectrum (300 MHz,  $\text{CD}_3\text{CN}$ , 25 °C):  $\delta = 168.33$  ( $\text{C}^4$ ), 159.45 ( $\text{C}^3$ ), 156.38 ( $\text{C}^5$ ), 150.55 ( $\text{C}^9$ ), 142.38 ( $\text{C}^1$ ), 140.68 ( $\text{C}^2$ ), 125.63 ( $\text{C}^7$ ), 122.71 ( $\text{C}^6$ ), 122.38 ( $\text{C}^8$ ) ppm.

**$[\text{Fe}(\text{L}^1)_2\text{--}\{\text{Cu}(\text{CH}_3\text{CN})_2\}](\text{ClO}_4)$  (**4**):** To a solution of  $\text{Et}_4\text{N}[\text{Fe}(\text{L}^1)_2]$  (**2**) (0.100 g, 0.122 mmol) in 20 mL of  $\text{CH}_3\text{CN}$ , solid  $[\text{Cu}(\text{CH}_3\text{CN})_4](\text{ClO}_4)$  (0.080 g, 0.243 mmol) was added under the magnetic stirring. The resultant deep-red coloured reaction mixture was stirred for 1 h. The solution was filtered and the volatiles were removed under reduced pressure. The resulting crude product was re-dissolved in  $\text{CH}_3\text{CN}$  and subjected to the vapor diffusion of diethyl ether. This afforded the red coloured crystalline product suitable for the structural analysis; yield: 0.082 g, 67%.  $\text{C}_{38}\text{H}_{28}\text{ClCu}_2$

$\text{FeN}_{12}\text{O}_8$  (999.09): calcd. C 45.68, H 2.82, N 16.82; found C 45.53, H 2.75, N 16.42. FTIR spectrum (KBr disk):  $\tilde{\nu} = 2293, 2253, 1628, 1595, 1098 \text{ cm}^{-1}$ . Conductivity ( $\text{CH}_3\text{CN}$ , ca. 1 mM solution, 298 K):  $\Lambda_{\text{M}} = 130 \text{ } \Omega^{-1}\text{cm}^2\text{mol}^{-1}$ . UV/Vis spectrum ( $\text{CH}_3\text{CN}$ ):  $\lambda_{\text{max}}$  ( $\epsilon$ ,  $\text{M}^{-1}\text{cm}^{-1}$ ): 440 (4770) nm.  $\mu_{\text{eff}}$  (DMF, 298 K, Evans' method): 4.7 BM.

**General Procedure for the Catalytic Oxidation of Sterically Hindered Phenols:** One of the substrate phenols was dissolved in  $\text{CH}_3\text{OH}$  (15 mL) under the dinitrogen atmosphere. The solid catalyst (5 mol-%) was then added under magnetic stirring and the mixture was exposed to dioxygen. The reaction was allowed to stir for ca. 6 h at room temperature. The progress of the reaction was monitored by TLC (5% EtOAc/hexane). Solvent was removed under the reduced pressure and the residue was triturated with  $\text{CH}_2\text{Cl}_2$ . The catalyst thus separated was filtered off. The filtrate was concentrated to afford the crude product which was purified by the column chromatography using 100–200 mesh silica and 1:1 EtOAc/hexane as the eluent. Products were identified by GC-MS and  $^1\text{H}$  NMR spectra.

**Physical Measurements:** The conductivity measurements were done in organic solvents using the digital conductivity bridge from the Popular Traders, India (model number: PT-825). The elemental analysis data were obtained from the Elementar Analysen Systeme GmbH Vario EL-III instrument. The NMR measurements were done using an Avance Bruker (300 MHz) instrument. The infra-red spectra (either as KBr pellet or as a mull in mineral oil) were recorded using a Perkin-Elmer FTIR 2000 spectrometer. The absorption spectra were recorded using the Perkin-Elmer Lambda-25 spectrophotometer. The mass spectra were obtained from the LC-TOF (KC-455) mass spectrometer of Waters. GC-MS studies were performed with Shimadzu instrument (QP-2010) with RTX-5SIL-MS column. Thermogravimetric analysis (TGA) and differential scanning calorimetry (DSC) were performed on DTG-60 SHIM-ADZU and TA DSC Q 200 instruments, respectively, at 5 °C/min heating rate under the nitrogen atmosphere. Solution magnetic susceptibility measurements were done by the Evans' method with a Hitachi R-600 FT NMR (60 MHz) spectrometer. The diamagnetic corrections were made as per the literature. The cyclic voltammetric experiments were performed by using a CH Instruments electrochemical analyzer (1120 A). The cell contained a glassy-carbon or platinum working electrode, a Pt wire auxiliary electrode, and a saturated calomel electrode (SCE) or  $\text{Ag}/\text{Ag}^+$  reference electrode. A salt bridge (containing supporting electrolyte, TBAP, dissolved in either MeCN or DMF) was used to connect the reference electrode with the experimental solution. The solutions were ca. 1 mM in complex and ca. 0.1 M in supporting electrolyte, TBAP. Under our experimental conditions, the  $E_{1/2}$  value (Volt units) for the couple  $\text{Fc}^+/\text{Fc}$  (ferrocenium/ferrocene couple) was found to be 0.40 V in MeCN vs. SCE.

**Crystal Structure Determination:** Single crystals suitable for the X-ray diffraction studies were grown by the vapor diffusion of diethyl ether to a  $\text{CH}_3\text{CN}$  solution for all complexes. The intensity data for complex **2** was collected at 293 K on a Oxford XCalibur CCD diffractometer equipped with graphite monochromatic  $\text{Mo-K}\alpha$  radiation ( $\lambda = 0.71073 \text{ \AA}$ ).<sup>[33]</sup> For complexes **3** and **4**, the intensity data were obtained at 100 K from a Bruker Kappa Apex-CCD diffractometer using graphite-monochromated  $\text{Mo-K}\alpha$  radiation ( $\lambda = 0.71073 \text{ \AA}$ ).<sup>[34,35]</sup> Intensity data were corrected for Lorentz polarization effects, and an empirical absorption correction (SADABS) was applied.<sup>[36]</sup> The structures were solved by the direct methods and refined by the full-matrix least-squares refinement techniques on  $F^2$  using the program SHELXL-97 in WinGX module.<sup>[37]</sup> All

Table 4. Crystallographic data collection and structural refinement parameters for complexes **2**, **3**, and **4**.

	<b>2</b>	<b>3</b>	<b>4</b>
Empirical formula	C <sub>84</sub> H <sub>86</sub> Fe <sub>2</sub> N <sub>22</sub> O <sub>9</sub>	C <sub>38</sub> H <sub>28</sub> CoN <sub>12</sub> O <sub>8</sub> ClCu <sub>2</sub>	C <sub>38</sub> H <sub>28</sub> FeN <sub>12</sub> O <sub>8</sub> ClCu <sub>2</sub>
Formula weight	1659.45	1002.18	999.10
Temp. [K]	293(2)	100(2)	100(2)
Crystal system	monoclinic	monoclinic	monoclinic
Space group	<i>P</i> 2 <sub>1</sub> / <i>n</i> 1	<i>P</i> 2 <sub>1</sub> / <i>n</i> 1	<i>P</i> 2 <sub>1</sub> / <i>n</i> 1
<i>a</i> [Å]	19.378(5)	10.087(3)	10.121(3)
<i>b</i> [Å]	22.610(5)	23.522(7)	23.691(6)
<i>c</i> [Å]	19.782(5)	16.955(5)	16.971(4)
<i>α</i> [°]	90	90	90
<i>β</i> [°]	111.525(5)	91.870(6)	91.355(4)
<i>γ</i> [°]	90	90	90
<i>V</i> [Å <sup>3</sup> ]	8063(3)	4020(2)	4068(17)
<i>Z</i>	4	4	4
<i>d</i> [g cm <sup>−3</sup> ]	1.367	1.656	1.631
Abs. coefficient [mm <sup>−1</sup> ]	0.433	1.592	1.522
<i>F</i> (000)	3472	2024	2020
<i>R</i> (int.)	0.0420	0.0919	0.0584
Final <i>R</i> indices [ <i>I</i> > 2σ( <i>I</i> )] <sup>[a]</sup>	<i>R</i> 1 = 0.0627; <i>wR</i> 2 = 0.1385	<i>R</i> 1 = 0.0685; <i>wR</i> 2 = 0.1601	<i>R</i> 1 = 0.0774; <i>wR</i> 2 = 0.1813
<i>R</i> indices (all data)	<i>R</i> 1 = 0.1246; <i>wR</i> 2 = 0.1663	<i>R</i> 1 = 0.1261; <i>wR</i> 2 = 0.2011	<i>R</i> 1 = 0.1054; <i>wR</i> 2 = 0.2002
GOF on <i>F</i> <sup>2</sup>	1.011	1.034	1.046

[a] *R*1 = Σ||*F*<sub>o</sub>| − |*F*<sub>c</sub>||/Σ|*F*<sub>o</sub>|; *wR*2 = {Σ[*w*(*F*<sub>o</sub><sup>2</sup> − *F*<sub>c</sub><sup>2</sup>)]/Σ[*wF*<sub>o</sub><sup>4</sup>]}<sup>1/2</sup>.

hydrogen atoms were fixed at the calculated positions with isotropic thermal parameters and all non-hydrogen atoms were refined anisotropically. The crystal structures of the complexes **3** and **4** have disorder and/or partial occupancy complication with ClO<sub>4</sub><sup>−</sup> anion. The occupancy of the chlorine atom of the ClO<sub>4</sub><sup>−</sup> anion was 0.5 and as a result asymmetric unit cell of the complexes **3** and **4** show two independent ClO<sub>4</sub><sup>−</sup> anions. The oxygen atoms attached to the chlorine atom of the ClO<sub>4</sub><sup>−</sup> anion also had occupancy disorders and thus were refined isotropically. Intermolecular interactions were examined with the DIAMOND 2.0 and 3.0 packages.<sup>[38]</sup> Details of the crystallographic data collection and structural solution parameter are given in Table 4.

CCDC-776045 (for **2**), -776046 (for **4**), and -776047 (for **3**) contain the crystallographic data for this paper. These data can be obtained free of charge from The Cambridge Data Center via [www.ccdc.ac.uk/data\\_request/cif](http://www.ccdc.ac.uk/data_request/cif).

**Supporting Information** (see also the footnote on the first page of this article): Packing diagram of complex **2**, absorption spectra of **1–4**, NMR spectra of **3**, DSC and TGA plots for **3** and **4**, and cyclic voltammograms of **3** and **4**.

## Acknowledgments

R. G. gratefully acknowledges the financial support from the Department of Science & Technology (DST), Government of India; crystallographic data collection from IIT–Kanpur and CIF facility of this university; and GC-MS facility from AIRF center of JNU, New Delhi. A. P. S. thanks the Council of Scientific and Industrial Research (CSIR), New Delhi for an SRF fellowship.

- [1] a) S. Kitagawa, R. Kitaura, S.-I. Noro, *Angew. Chem. Int. Ed.* **2004**, *43*, 2334; b) C. Janiak, *Dalton Trans.* **2003**, 2781; c) N. L. Rosi, J. Eckert, M. Eddaoudi, D. T. Vodak, J. Kim, M. O’Keeffe, O. M. Yaghi, *Science* **2003**, *300*, 1127; d) O. M. Yaghi, M. O’Keeffe, N. W. Ockwig, H. K. Chae, M. Eddaoudi, J. Kim, *Nature* **2003**, *423*, 705; e) H. K. Chae, D. Y. Siberio-Perez, J. Kim, Y. Go, M. Eddaoudi, A. J. Matzger, M. O’Keeffe, O. M. Yaghi, *Nature* **2004**, *427*, 523; f) S.-I. Noro, R. Kitaura, M. Kondo, S. Kitagawa, T. Ishii, H. Matsuzaka, M. Yamashita, *J. Am. Chem. Soc.* **2002**, *124*, 2568; g) L. Pan, H. Liu, X. Lei, X. Huang, D. H. Olson, N. J. Turro, J. Li, *Angew. Chem. Int. Ed.* **2003**, *42*, 542; h) S. Kitagawa, K. Uemura, *Chem. Soc. Rev.* **2005**, *34*, 109; i) S. L. James, *Chem. Soc. Rev.* **2003**, *32*, 276; j) B. Kesanli, W. Lin, *Coord. Chem. Rev.* **2003**, *246*, 305; k) G. Ferey, C. Mellot-Draznieks, C. Serre, F. Millange, *Acc. Chem. Res.* **2005**, *38*, 217; l) E. Y. Lee, S. Y. Jang, M. P. Suh, *J. Am. Chem. Soc.* **2005**, *127*, 6374; m) M. Yoshizawa, J. K. Klosterman, M. Fujita, *Angew. Chem.* **2009**, *48*, 3418; n) G. Ferey, *Chem. Soc. Rev.* **2008**, *37*, 191.
- [2] a) B. Kesanli, W. Lin, *Coord. Chem. Rev.* **2003**, *246*, 305; b) C. J. Shorrock, H. Jong, R. J. Batchelor, D. B. Leznoff, *Inorg. Chem.* **2003**, *42*, 3917; c) T. J. Burchell, R. J. Puddephatt, *Inorg. Chem.* **2005**, *44*, 3718; d) M. Sarkar, K. Biradha, *Cryst. Growth Des.* **2007**, *7*, 1318; e) D. K. Kumar, A. Das, P. Dastidar, *CrystEngComm* **2006**, *8*, 805; f) R. A. Fischer, C. Woll, *Angew. Chem. Int. Ed.* **2008**, *47*, 8164; g) E. Pardo, R. Ruiz-García, J. Cano, X. Ottenwaelde, R. Lescouezec, Y. Journaux, F. Lloret, M. Julve, *Dalton Trans.* **2008**, 2780; h) R. Ganguly, B. Sreenivasulu, J. J. Vittal, *Coord. Chem. Rev.* **2008**, *252*, 1027; S. J. Lee, J. T. Hupp, *Coord. Chem. Rev.* **2006**, *250*, 1710.
- [3] a) S. Leininer, B. Olenyuk, P. J. Stang, *Chem. Rev.* **2000**, *100*, 853; b) S. R. Seidel, P. J. Stang, *Acc. Chem. Res.* **2002**, *35*, 972; c) M. Sarkar, K. Biradha, *Chem. Commun.* **2005**, 2229; d) S. L. James, *Chem. Soc. Rev.* **2003**, *32*, 276; e) J. A. Thomas, *Chem. Soc. Rev.* **2007**, *36*, 856; f) S. J. Dalgarno, N. P. Power, J. L. Atwood, *Coord. Chem. Rev.* **2008**, *252*, 825; g) D. Tanaka, S. Kitagawa, *Chem. Mater.* **2008**, *20*, 922; h) N. Das, P. S. Mukherjee, A. M. Arif, P. J. Stang, *J. Am. Chem. Soc.* **2003**, *125*, 13950; i) P. S. Mukherjee, N. Das, P. J. Stang, *J. Org. Chem.* **2004**, *69*, 3526; j) P. S. Mukherjee, N. Das, Y. Kryschenko, A. M. Arif, P. J. Stang, *J. Am. Chem. Soc.* **2004**, *126*, 2464.
- [4] K. Biradha, M. Sarkar, L. Rajput, *Chem. Commun.* **2006**, 4169, and references cited therein.
- [5] a) S. R. Halper, L. Do, J. R. Stork, S. M. Cohen, *J. Am. Chem. Soc.* **2006**, *128*, 15255; b) S. J. Garibay, J. R. Stork, Z. Wang, S. M. Cohen, S. G. Telfer, *Chem. Commun.* **2007**, 4881; c) J. R. Stork, V. S. Thoi, S. M. Cohen, *Inorg. Chem.* **2007**, *46*, 11213; d) B. Chen, F. R. Fronczek, A. W. Maverick, *Inorg. Chem.* **2004**, *43*, 8209; e) B. Chen, F. R. Fronczek, A. W. Maverick, *Chem. Commun.* **2003**, 2166; f) Y. Zhang, B. Chen, F. R. Fronczek, A. W. Maverick, *Inorg. Chem.* **2008**, *47*, 4433; g) V. D. Vreshch, A. N. Chernega, J. A. K. Howard, J. Sielder, K. V. Domasevitch, *Dalton Trans.* **2003**, 1707.



- [6] D. J. Tramchemotgne, J. L. Mendoza-Cortes, M. O'Keeffe, O. M. Yaghi, *Chem. Soc. Rev.* **2009**, 38, 1257.
- [7] A. Ali, A. P. Singh, R. Gupta, *J. Chem. Sci.* **2010**, 122, 311, and references cited therein.
- [8] A. Mishra, A. Ali, S. Upreti, R. Gupta, *Inorg. Chem.* **2008**, 47, 154.
- [9] A. Mishra, A. Ali, S. Upreti, M. S. Whittingham, R. Gupta, *Inorg. Chem.* **2009**, 48, 5234.
- [10] A. Mishra, N. K. Kaushik, A. K. Verma, R. Gupta, *Eur. J. Med. Chem.* **2008**, 43, 2189.
- [11] K. Nakamoto, in: *Infrared and Raman Spectra of Inorganic and Coordination Compounds*, John Wiley & Sons, New York, **1986**.
- [12] W. J. Geary, *Coord. Chem. Rev.* **1971**, 7, 81.
- [13] D. F. Evans, *J. Chem. Soc.* **1959**, 2003.
- [14] A. P. Singh, N. K. Kaushik, A. K. Verma, G. Hundal, R. Gupta, *Eur. J. Med. Chem.* **2009**, 44, 1607.
- [15] a) N. Kitajima, T. Koda, Y. Iwata, Y. Moro-oka, *J. Am. Chem. Soc.* **1990**, 112, 8833; b) A. M. Guidote Jr., K.-I. Ando, K. Terada, Y. Kurusu, H. Nagao, Y. Masuyama, *Inorg. Chim. Acta* **2001**, 324, 203; c) B. Lucchese, K. J. Humphreys, D.-H. Lee, C. D. Incarvito, R. D. Sommer, A. L. Rheingold, K. D. Karlin, *Inorg. Chem.* **2004**, 43, 5987; d) V. Mahadevan, J. L. DuBois, B. Hedman, K. O. Hodgson, T. D. P. Stack, *J. Am. Chem. Soc.* **1999**, 121, 5583; e) M. Matsushita, K. Kamata, K. Yamaguchi, N. Mizuno, *J. Am. Chem. Soc.* **2005**, 127, 6632.
- [16] a) L. I. Simandi, *Catalytic Activation of Dioxygen by Metal Complexes*, Kluwer, Amsterdam, **1992**; b) G. A. Hamilton, in: *Molecular Mechanism of Dioxygen Activation* (Ed.: O. Hayashi), Academic Press, New York, **1974**, p. 405; c) R. A. Sheldon, J. K. Kochi, *Metal Catalysed Oxidations of Organic Compounds*, Academic Press, New York, **1981**.
- [17] A. E. Martell, D. T. Sawyer (Eds.), *Oxygen Complexes and Oxygen Activation by Transition Metals*, Plenum Press, New York, **1987**.
- [18] K. P. Ross, E. I. Solomon, *J. Am. Chem. Soc.* **1991**, 113, 3246, and references cited therein.
- [19] H. L. Finkbeiner, A. S. Hay, D. M. White, *Polymerization Processes* (Eds.: C. E. Schildknecht, I. Skeist), Wiley-Interscience, New York, **1977**, pp. 537.
- [20] G. Pandey, C. Muralikrishna, U. T. Bhalerao, *Tetrahedron Lett.* **1990**, 31, 3771.
- [21] R. Gupta, R. Mukherjee, *Tetrahedron Lett.* **2000**, 41, 7763 and references cited therein.
- [22] M. Gupta, S. K. Upadhyay, M. A. Sridhar, P. Mathur, *Inorg. Chim. Acta* **2006**, 359, 4360.
- [23] P. Mulder, S. Hemmink, M. I. De Heer, M. Lupo, D. Santoro, H.-G. Korth, *J. Org. Chem.* **2001**, 66, 6611.
- [24] F. G. Bordwell, J.-P. Cheng, G.-Z. Ji, A. V. Satish, X. Zhang, *J. Am. Chem. Soc.* **1991**, 113, 9790.
- [25] G. F. Peduli, M. Lucarini, P. Pedrielli, S. Fattuoni, *J. Org. Chem.* **1996**, 61, 9259.
- [26] N. Kitajima, Y. Moro-oka, *Chem. Rev.* **1994**, 94, 737.
- [27] S. K. Sharma, S. Upreti, R. Gupta, *Eur. J. Inorg. Chem.* **2007**, 3247.
- [28] J. Singh, G. Hundal, R. Gupta, *Eur. J. Inorg. Chem.* **2008**, 2052.
- [29] J. Singh, G. Hundal, R. Gupta, *Eur. J. Inorg. Chem.* **2009**, 3259.
- [30] S. K. Sharma, S. Upreti, R. Gupta, *Eur. J. Inorg. Chem.* **2010**, 621.
- [31] J. Singh, G. Hundal, M. Corbella, R. Gupta, *Polyhedron* **2007**, 26, 3893.
- [32] a) K. S. Hagen, *Inorg. Chem.* **2000**, 39, 5867; b) G. Kubas, *Inorg. Synth.* **1979**, 19, 90; c) G. Kubas, *Inorg. Synth.* **1990**, 28, 68.
- [33] *CrysAlisPro*, Oxford Diffraction Ltd., version 1.171.33.49b, **2009**.
- [34] *SMART: Bruker Molecular Analysis Research Tool*, version 5.618, Bruker Analytical X-ray System, **2000**.
- [35] *SAINT-NT*, version 6.04, Bruker Analytical X-ray System, **2001**.
- [36] *SHELXTL-NT*, version 6.10, Bruker Analytical X-ray System, **2000**.
- [37] L. J. Farrugia, *WinGX*, version 1.64, *An Integrated System of Windows Programs for the Solution, Refinement and Analysis of Single-Crystal X-ray Diffraction Data*, Department of Chemistry, University of Glasgow, **2003**.
- [38] *DIAMOND*, version 2.1c, Crystal Impact GbR, Bonn, Germany, **1999**.

Received: May 18, 2010

Published Online: August 16, 2010